Two features at the two-dimensional freezing transitions

Ziren Wang,[1] Weikai Qi,[2] Yi Peng,[1] Ahmed M. Alsayed,[3,4] Yong Chen,[2] Penger Tong,[1] and Yilong Han[1,a)]

[1]*Department of Physics, Hong Kong University of Science and Technology, Clear Water Bay, Hong Kong, China*
[2]*Institute of Theoretical Physics, Lanzhou University, Lanzhou 730000, China*
[3]*Department of Physics and Astronomy, University of Pennsylvania, 209 South 33rd St., Philadelphia, Pennsylvania 19104, USA*
[4]*Complex Assemblies of Soft Matter, CNRS/UPENN/Rhodia UMI 3254, Bristol, Pennsylvania 19007, USA*

(Received 20 September 2010; accepted 4 January 2011; published online 20 January 2011)

We studied the two-dimensional freezing transitions in monolayers of microgel colloidal spheres with short-ranged repulsions in video-microscopy experiments, and monolayers of hard disks, and Yukawa particles in simulations. These systems share two common features at the freezing points: (1) the bimodal distribution profile of the local orientational order parameter; (2) the two-body excess entropy, s_2, reaches $-4.5 \pm 0.5\,k_B$. Both features are robust and sensitive to the freezing points, so that they can potentially serve as empirical freezing criteria in two dimensions. Compared with the conventional freezing criteria, the first feature has no finite-size ambiguities and can be resolved adequately with much less statistics; and the second feature can be directly measured in macroscopic experiments without the need for microscopic information. © *2011 American Institute of Physics*. [doi:10.1063/1.3545967]

I. INTRODUCTION

Empirical criteria for melting and freezing have been proved important for assigning phase transition points[1,2] because free energies are often not directly measurable in many experimental systems. One famous example is the Lindemann criterion[3] which has been widely used in three-dimensional (3D) melting. For two-dimensional (2D) freezing, the following five phenomenological criteria have been proposed: (1) the 2D version of the Hansen–Verlet (HV) freezing rule,[4] (2) the 2D dynamic Löwen–Palberg–Simon (LPS) criterion,[5,6] (3) the split of the second peak of the radial distribution function,[7,8] (4) the bimodal distribution profile of the shape factor of Voronoi polygons,[9] and (5) the zero residual multiparticle entropy (zero-RMPE) criterion.[10] Criteria (1) and (2) have been tested in both equilibrium and nonequilibrium simulations[11] with various particle interactions. Criterion (3) has a 5% ambiguity around the freezing points for hard disks,[8] Lennard-Jones systems[7] and colloidal microgel spheres with short-range repulsions.[12] Criterion (4) consistently underestimates the freezing points for hard disks[9,13] and microgels by 6% volume fractions.[12] Criterion (5) has been tested in hard disks,[14] 2D and 3D Lennard-Jones systems[14,15] and even rods at nematic–smectic transitions in 3D,[16] but was found to be more ambiguous in systems with short-range repulsions,[17] and attractions[15] at high densities.[18] Recently, we have observed two new features at the freezing point of a monolayer of microgel spheres, namely, the divergent peak of the orientational susceptibility and the percolation of caged particles.[12] These two features could potentially be used as new criteria for 2D freezing if they hold universally for various particle interactions.

Besides empirical criteria, fundamental theories have been formulated for 2D melting.[19–22] However these theories apply to single-crystal melting without surface or grain-boundary effects, and so often cannot be applied directly to freezing experiments. In practice, homogenous nucleation during the freezing often produces polycrystalline solids, whose grain boundaries break both the translational and orientational orders studied in 2D melting theories. Such polycrystals certainly have no hexatic phase predicted by Kosterlitz-Thouless-Halperin-Nelson-Young (KTHNY) theory because grain boundaries break all the possible long or quasilong ranged orders. In contrast, the empirical freezing criteria remains valid in polycrystalline freezing.[12]

2D freezing has been experimentally studied in colloids,[23,24] dusty plasmas,[25,26] and driven granular systems.[13] These experiments focused on local structures, dynamics, and the initial nucleation processes rather than the freezing criteria. Recently, some of us experimentally tested the freezing criteria (1)–(4) in a thermal system for the first time.[12] In the current study, we observed two more new features at the freezing points of this experimental system[12] and two simulation systems with different particle interactions. Hence the two features could serve as new freezing criteria, if they universally hold in all systems.

II. EXPERIMENTAL AND SIMULATION SYSTEMS

The experiment employed isopropyl acrylamide (NIPA) microgel spheres whose diameters can be temperature tuned.[27] Thus the freezing or melting transition can be driven by a modeterate temperature change in a single sample.[28,29] The NIPA spheres were sterically stabilized and the electrostatic repulsion between these weakly charged spheres was

a)Electronic mail: yilong@ust.hk.

negligible in the aqueous buffer solution. The softness of the particles yields short-range repulsive pair potentials.[29] The pair potentials were directly quantified by measuring the radial distribution function, $g(r)$, in a dilute (i.e., area density $\rho \sim 10\%$) monolayer of spheres,[30–32] and the small bright-field image artifact due to the image overlap of adjacent particles[33] has been corrected by the method described in Ref. 32. The diameters of soft particles are ambiguous. Here we define the effective diameter σ as $u(\sigma) = 1k_BT$, and the area fraction $\rho = \rho_n \pi \sigma^2/4$ where ρ_n is the number density. The measured effective diameter of the NIPA spheres varied linearly from 0.71 μm at 29.5 °C to 0.92 μm at 24.1 °C. The sample consisted of a monolayer of NIPA spheres confined between two parallel glass slides, see the details in Ref. 12. The uniform monolayer of spheres nucleated homogenously, and flows were not detected during the experiment. The thermal motions of particles were observed under a microscope with a 100× objective and recorded by a 14-bit low-noise charge-coupled device (CCD) camera at 3.57 frames/s. Each frame contained about 23 000 spheres in a 1392 × 1040 pixels (i.e., 147.3 × 110.2μm^2) field of view. The temperature control on the microscope had a resolution of 0.1 °C. We decreased the temperature from 29.5 to 24.1°C at a rate of 0.3 °C/step and recorded 20 min video at each temperature after 10 min of equilibration. Waiting a few minutes or 1 h for equilibration appeared to produce little difference since the temperature change is only 0.3 °C. The particle positions in each frame were identified using the standard image analysis algorithms.[34]

Besides the experiments, we performed two simulations with different particle interactions. The first one was an event-driven molecular dynamics (MD) simulation of 22 500 hard disks. The particle number chosen for the simulation is very close to the actual particle number obtained in the experiment. In contrast to the polycrystalline solids in the experiments, the hard disks in the simulation homogenously froze into a single crystal due to the slow quenching rate, the small system size, and the periodic boundary condition. The area fraction ρ was changed from 0.754 to 0.660 at 0.0785/step. Note that temperature is not defined in hard-disk systems so that only area fraction is used to characterize them.

The second simulation was a Brownian dynamics (BD) simulation of 22 500 particles with a Yukawa pair potential.[35] The Yukawa potential, i.e., the screened-Coulomb potential, characterizes the interaction between charge-stabilized colloidal particles.[36] It is defined as

$$u(r) = U_0 \frac{r_0}{r} \exp\left(-\lambda \frac{r - r_0}{r_0}\right), \tag{1}$$

where U_0 is the energy scale, r_0 is the length scale, r is the distance between particles, and λ is the screening parameter. We set $\lambda = 8$, $U_0 = 1$, $\sigma = 1.0$, $\rho_n = N/V = 1.0$, and $T^* = k_BT/U_0$ in the reduced unit. In our simulation, r_0, U_0, ρ, and λ were fixed and the reduced temperature, T^*, was changed from 0.70 to 0.52 at 0.03/step (area fraction from 0.849 to 0.904 at ~0.01/step). In this temperature range, the potential is rather soft, see Fig. 1. We performed the standard BD simulation which is based on the Langevin equation

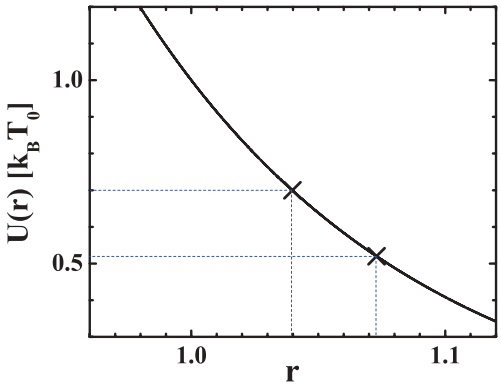

FIG. 1. The Yukawa potential used in our Brownian dynamic simulation. The effective diameter σ changed from 1.04 at the reduced temperature $T^* = 0.70$–1.07 at $T^* = 0.51$.

of particle i

$$\xi \dot{\mathbf{r}}_i(t) = \mathbf{F}_i(t) + \mathbf{R}(t), \tag{2}$$

where $i = 1, \ldots, N$ labels the N particles. The friction coefficient $\xi = 1$ in the reduced unit, $\mathbf{R}(t)$ is the random thermal force in the solvent, and $\mathbf{F}_i(t)$ is the total interparticle force on particle i. The hydrodynamic interactions were ignored. Particles homogenously froze into a single crystal in a box with aspect ratio of $2 : \sqrt{3}$ under the periodic boundary condition. The time step $dt = 0.001\tau$ where $\tau = \sigma^2\xi/U_0$ was the time scale used in the simulation. The system usually reached equilibrium after 10–20τ and the data were typically acquired during 50–60τ. Around the freezing point, the equilibration time was longer so that the data were acquired during 110–120τ.

III. FREEZING POINTS ASSIGNMENT

We identified the freezing transition point with the traditional 2D HV freezing rule [criterion (1)] and the divergence of the susceptibility. The HV freezing rule states that a 2D liquid freezes when the amplitude of the first peak of the structure factor, $S(k)$, exceeds a critical value of approximately five. For different particle interactions, this critical value varies from 4.4 to 5.5.[4,7,37] Despite this ambiguity, the freezing point can usually be accurately identified because the amplitude of the first peak changes rapidly around the freezing point.

The divergence of the susceptibility is a feature associated with the phase transition[38] rather than being just an empirical feature. The 2D freezing transition corresponds to the divergence of the susceptibility of the orientational order parameter.[12] The local orientational order parameter[20,39] of particle i is

$$\psi_{6i} = \frac{1}{nn_i} \sum_{j=1}^{nn_i} e^{6i\theta_{ij}}, \tag{3}$$

where θ_{ij} is the angle of the bond between particle $i$and its neighbor j. nn_i is the number of the nearest neighbors identified from the Delaunay triangulation. The global orientational order parameter $\psi_6 = \langle \psi_{6i} \rangle = (\sum_{i=1}^{N} \psi_{6i})/N$ is the average of the local order parameters over all N particles. ψ_6 characterizes the sixfold symmetry in 2D. $\psi_6 = 1$ for a perfect

triangular lattice, and $\psi_6 = 0$ for a random liquid. The orientational susceptibility

$$\chi_6 = \lim_{A\to\infty} A\left(\langle|\psi_6^2|\rangle - \langle|\psi_6|\rangle^2\right), \quad (4)$$

is the time fluctuation of the global orientational order parameter ψ_6 in area A. We calculated χ in different sized sub-areas and extrapolated to the infinite-size limit.[29] Without such extrapolation, the freezing point can still be correctly measured since the position of the divergence peak is robust for areas of different sizes as long as the area is not too small. Hence the χ_6 criterion has less finite-size ambiguities[29] and does not depend on an empirical critical value as do the freezing criteria (1), (2), and (5).

Besides using the above two methods to assign the freezing points, we also calculated the freezing criterion (3) which states that the second peak of the radial distribution function, $g(r)$, develops a shoulder at the freezing point. Although this criterion is less accurate,[7,8,12] we measured it since $g(r)$ was also used in the measurement of the excess entropy as described in Sec. V.

Figures 2–4[(a)–(c)] show the results of the 2D HV freezing rule, the susceptibilities and the radial distribution functions in the five systems, respectively. The three criteria yielded almost consistent results except for Yukawa particles. The Yukawa potential in Fig. 1 was very soft so that the second peak of $g(r)$ is smeared out at the freezing point in Fig. 4(c). The obtained freezing points were 27.7 °C ($\rho = 0.747$) for the NIPA-freezing experiment; $\rho = 0.683$ for the hard-disk simulation; the reduced temperature $T^* = 0.61$ ($\rho = 0.874$) for the Yukawa-particle simulation. These area fractions are comparable to the freezing points of 0.695 ± 0.003 for hard disks,[40–43] 0.77 for r^{-12}-potential particles[4] and 1.188 for r^{-6}-potential particles.[44] The trend of softer particles with higher freezing area fractions can be clearly resolved.

We did not use the other criteria to assign the freezing points because they are either not always measurable or not accurate in our systems. The 2D LPS freezing criterion

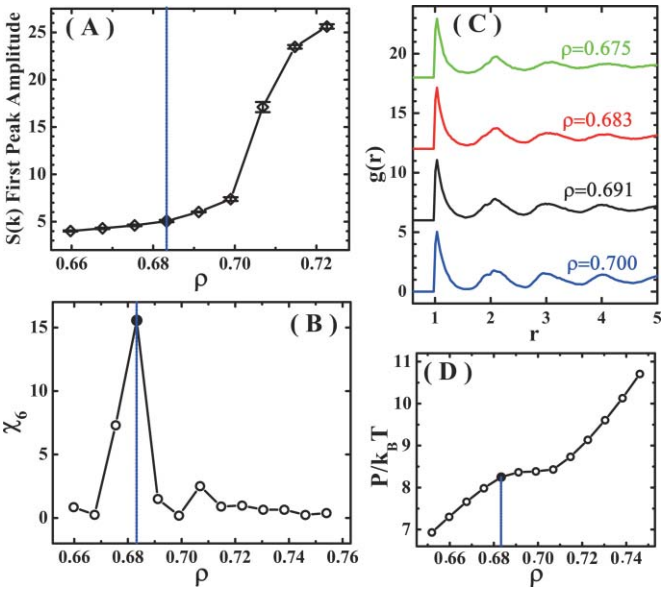

FIG. 3. The MD simulation of the freezing of hard disks. (A) The first-peak amplitudes of the structure factors at different temperatures. According to the 2D HV freezing criterion, the freezing point is near the area fraction 0.683. (B) Orientational susceptibilities at different temperatures. The position of the peak corresponds to the freezing point of 0.683. (C) The radial distribution functions. (D) The equation of state. The van der Waals loop indicates that the freezing area fraction is around 0.683.

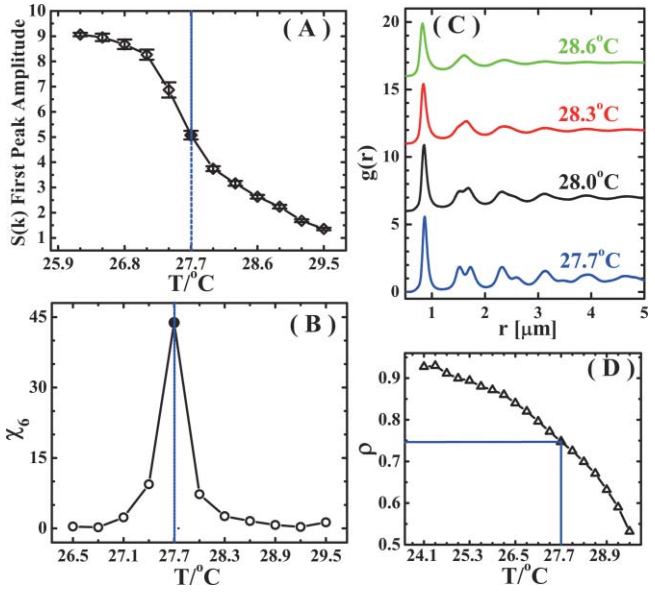

FIG. 2. Freezing of a monolayer of NIPA spheres. (A) The first-peak amplitude of the structure factors, $S(k)$, at different temperatures. According to the 2D HV freezing criterion, the freezing point is at 27.7°C. (B) Orientational susceptibilities at different temperatures. The position of the peak corresponds to the freezing point of 27.7 °C. (C) The radial distribution functions. The split of the second peak corresponds to the freezing point. (D) The area fraction as a function of temperature.

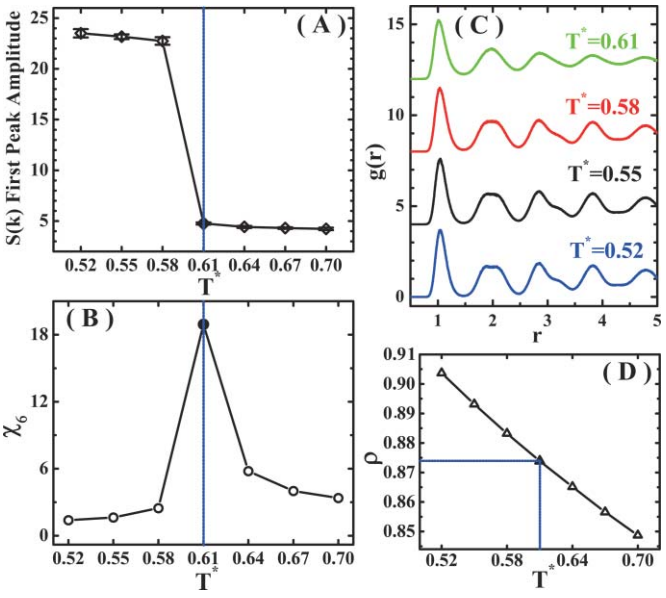

FIG. 4. The BD simulation of the freezing of Yukawa disks. (A) The first-peak amplitudes of the structure factors at different temperatures. According to the 2D HV freezing criterion, the freezing point is near the reduced temperature 0.60. (B) Orientational susceptibilities at different temperatures. The position of the peak corresponds to the freezing point of 0.61. (C) The radial distribution functions. (D) The area fraction as a function of temperature.

[criterion (2)] states that a 2D liquid freezes when the ratio of the averaged long-time diffusion coefficient to the averaged short-time diffusion coefficient is larger than a critical value ranging between 0.07 and 0.1, depending on particle interaction.[6,45] In contrast to other static criteria, this is a dynamic criterion for Brownian particles. However the diffusions at short-time and long-time limits span a large time scale which cannot be measured easily in MD and BD simulations and some of the video-microscopy experiments. Criterion (4) states that the shape factors of Voronoi polygons defined in Ref. 9 exhibit a bimodal distribution profile at the freezing point. The criterion appeared to underestimate the freezing points by 6%.[9,12,13] Criterion (5) regarding the residual multiparticle entropy is difficult to measure because it involves many-body correlations (see Sec. V for more details). One candidate freezing criterion suggested in Ref. 12 states that the caged particles percolate at the freezing transition. A particle is defined as caged if it cannot slip out of the triangle of three of its neighbors, see Refs. [12 and 46]. Hence the caging depends on the definition of the diameter which is somewhat ambiguous for soft spheres. If we use the effective diameter σ defined as $u(\sigma) = 1k_BT$, then the caged particles percolate within 5% of the volume fraction around the melting points in all the systems. Hence this criterion roughly holds. Here we suggest two new freezing criteria in Secs. IV and V, respectively. They are more accurate, less ambiguous, and easier to measure.

IV. BIMODAL DISTRIBUTION OF THE ORDER PARAMETER

We observed two common features shared by the five systems at their freezing points. The first feature is the bimodal distribution of the order parameter. The 2D local order parameter defined in Eq. (3) characterizes the sixfold orientational order of particle i relative to its nearest neighbors, i.e., the first-layer neighbors. In practice, however, $|\psi_{6i}|$ does not provide sufficient information to distinguish unambiguously between crystal-like and fluidlike particles,[47] hence a slightly different order parameter

$$n_{6i} = |\psi_{6i}^{*}\langle\psi_{6j}\rangle_j|, \tag{5}$$

was introduced.[47] The subscript j represents a first-layer neighbor of particle i. $\langle\ \rangle_j$ is the average over all first-layer neighbors of particle j. Hence this order parameter involves the neighbors of the neighbors and reflects the orientational order in two layers of neighbors. n_{6i} ranges between 0 and 1. A solidlike particle has more ordered neighbors so that its n_{6i} is close to 1, while a liquidlike particle has more disordered neighbors so that its n_{6i} is close to 0. In Fig. 5(a), the distributions of n_{6i} exhibit a peak near 1 in the solid phase, a peak near 0 in the liquid phase, and a bimodal profile at 27.7 °C which is exactly the freezing point identified in Fig. 2.

This bimodal distribution at the freezing point exists in all five systems as shown in Fig. 5. In Fig. 5, black circles denote the freezing points, triangles denote the liquids and squares denote the solids next to the freezing points. The histograms of n_{6i} in Fig. 5(c) do not have a bimodal distribution, which suggests that the freezing point is between

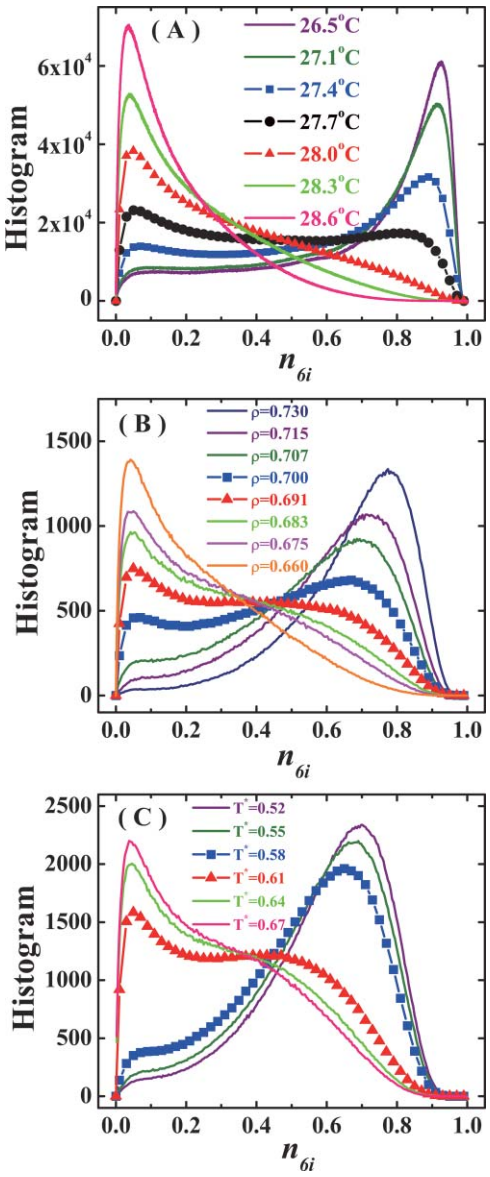

FIG. 5. The distributions of the orientational order parameter n_{6i}. (A) The NIPA-freezing experiment. The bimodal profile emerges at the freezing point 27.7 °C obtained in Fig. 2. (B) The hard-disk simulation. The bimodal profile emerges between the area fractions $\rho = 0.691$ and 0.700. (C) The Yukawa-particle simulation. The bimodal profile emerges at the reduced temperature $T^* = 0.60$ which is close to the freezing point obtained in Fig. 4.

25.6 °C ($\rho = 0.769$) and 25.8 °C ($\rho = 0.754$). This is in excellent agreement with the melting point from the 2D HV criterion in Fig. 3 which is also slightly below 25.8 °C. Among the five systems, the hard disks exhibit the largest discrepancy of only ~1% area fraction, see Fig. 5(d). In Fig. 5(d), the freezing point is between the area fractions 0.69 and 0.70, which is 1% higher than the 0.683 obtained in Fig. 3, but closer to the freezing point of 0.695 ± 0.003 in the literatures.[40–43] Our underestimated freezing point from Fig. 3 could be due to the finite-size effect. Here n_{6i} is a local parameter so that the area of the system does not affect its histogram profile. In contrast, the 2D HV freezing rule needs a large area for the small reciprocal lattice vector, $\mathbf{k}$, at the first peak of $S(|\mathbf{k}|)$. Hence the freezing point of $\rho = 0.695 \pm 0.005$ from the bimodal distribution in Fig. 5(d) might be more accurate

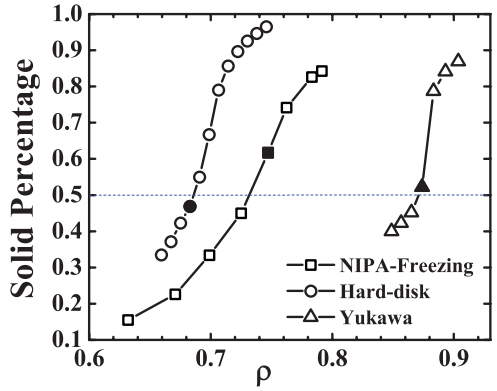

FIG. 6. The percentages of solid particles defined in Eq. (6) as a function of area fraction for the three systems. The solid symbols represent the freezing points resolved from Figs. 2 to 4. They are close to the 50% fraction indicated by the dotted horizontal line.

than the freezing point estimated from Fig. 3. Moreover, we observed that the histograms of n_{6i} need 5–10 times less statistics than the other criteria.

n_{6i} was originally used to distinguish solidlike and liquidlike particles. The solidlike particles are defined by the empirical criterion[47]

$$n_{6i} + |\psi_{6i}| > 1. \tag{6}$$

We found that about 50% of the particles became solidlike at the freezing point in all three systems, see Fig. 6. More details are shown in the joint distribution of $|\psi_{6i}|$ and n_{6i} in Fig. 7. In the solid phase, most particles are solidlike and are above the $n_{6i} + |\psi_{6i}| = 1$ line, while in the liquid phase, most particles are below this line. This feature in the joint distribution of $|\psi_{6i}|$ and n_{6i} has been observed in the experiments of charge-stabilized polystyrene (PS) spheres[47] and uncharged polymethylmethacrylate (PMMA) spheres.[48] At the freezing point of 27.7 °C, both the solidlike and liquidlike particles are

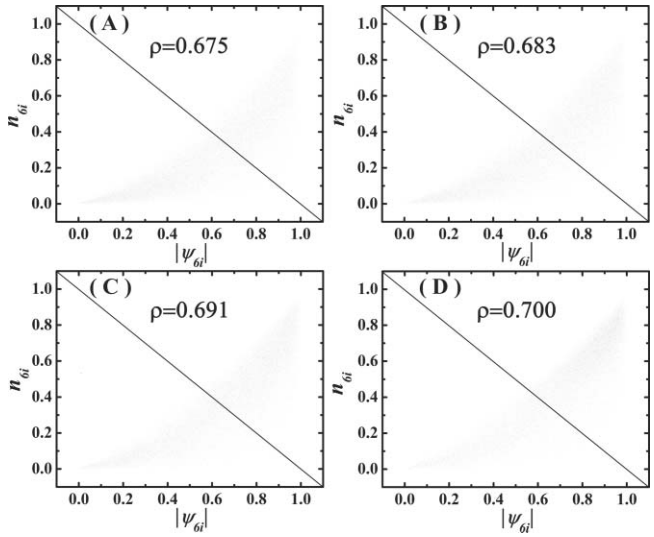

FIG. 7. The scatter plots of the joint distributions of the first-layer orientational order parameter ψ_{6i} and the two-layer orientational order parameter n_{6i} in the hard-disk simulation at area fraction (A) 0.675, (B) 0.683, (C) 0.691, (D) 0.700.

about 50%, which is another common feature at the freezing points across all three systems. This feature can be resolved with even less statistics, about one fifth of the statistics used in the bimodal histograms and about one fortieth of the statistics used in other criteria.

V. TWO-BODY EXCESS ENTROPY

The thermodynamic entropy of a system can be written as

$$S = S_1 + S_2 + S_3 + \ldots = S_1 + S_{ex}, \tag{7}$$

where S_n is the entropy contribution due to the n-particle spatial correlation.[49] The excess entropy, S_{ex}, is defined as the difference between the true entropy of the system S and that of the ideal gas S_1. The leading term in S_{ex} is the two-body excess entropy S_2. For example, S_2 contributes ~90% of S_{ex} for the Lennard-Jones system over a wide range of densities.[50] S_2 can be evaluated from the pair correlation function. For a 2D homogeneous system, S_2per particle is given by[50,51]

$$s_2 = S_2/N = -\pi k_B \rho_n \int_0^\infty [g(r)\ln g(r) - g(r) + 1] r dr, \tag{8}$$

where ρ_n is the number density. The integration above ten diameters contributes little so that our measured $g(r > 30\sigma)$ have long enough range to result in an accurate s_2. We observed that s_2 reaches $-4.5 \pm 0.5 k_B$ at the freezing points in all five systems, see Fig. 8. Here the $0.5\,k_B$ uncertainty corresponds to only 1% in area fraction since the slopes are steep near the freezing points. Above the freezing volume fractions, $s_2$decreases rapidly which reflects the much stronger two-body effect and a more limited range of neighbor separations. Note that $\ln g(r) = \ln[1 + (g(r) - 1)] \approx g(r) - 1$ when $g(r) \approx 1$, so that $s_2 \approx -\pi k_B \rho_n \int (g(r) - 1)^2 r dr$.[52] This expression is similar to the translational order parameter $t \equiv \int_0^\infty |g(\xi) - 1| d\xi$ where $\xi = r\rho_n^{1/3}$.[52–54] $t$quantifies the degree to which two neighboring particles adopt preferential separations.[53] Hence the large $|s_2|$above the freezing area fraction reflects a more ordered structure with uniform neighbor distances.

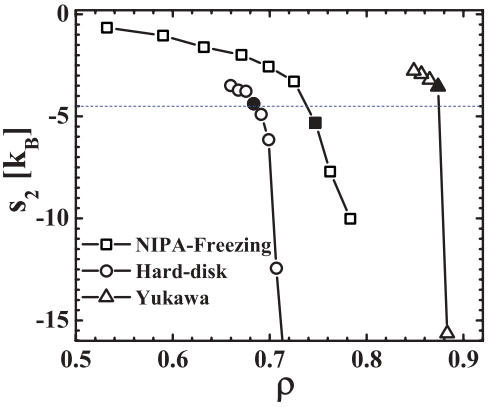

FIG. 8. Two-body excess entropy, s_2, as a function of area fraction ρ in the three systems. The solid symbols represent the freezing points that are close to $s_2 = -4.5 k_B$ as indicated by the horizontal dotted line.

Interestingly $s_2 = -4.5k_B$ has also been observed at the freezing point of 3D hard spheres.[53] Moreover we found that $s_2 = -4.5 \pm 0.5\ k_B$ also holds at the freezing points of multilayer thin films studied in Ref. 55 if we estimate s_2 from Eq. (8) and the measured in-plane $g(r)$. Spheres confined between two walls exhibit a cascade of phases: $1\triangle - 2 - 2\triangle - 3 - 3\triangle - 4 \cdots$ as the wall separation increases.[56] Here $n\triangle$ denotes an n-layer triangular lattice, and n denotes an n-layer square lattice. Both triangular and square lattices freeze at $s_2 \approx -4.5k_B$ in thin NIPA colloidal films. Hence we suggest that this feature could serve as a new freezing criterion.

This criterion is practically useful because s_2 can be obtained from either the pair correlation function using optical microscopy or the structure factor measured in a scattering experiment. The HV freezing criterion and $g(r)$-shoulder criterion can also be used in macroscopic experiments, while other freezing criteria require microscopic information of individual particles which limits their practical applications. Both the s_2 criterion and $g(r)$-shoulder criterion are based on $g(r)$, but the s_2 criterion yielded more accurate freezing points in our systems. Note that s_2 is integral quantity over the full range of $g(r)$, while the shoulder of the second peak in criterion (3) only reflects a local structural change in $g(r)$ and thus is less accurate for the soft Yukawa potential.

The s_2 criterion is similar to the zero-RMPE freezing rule [criterion (5)].[10] RMPE $\equiv s_{ex} - s_2$, which is the entropy, arose from three-body and higher order correlations. The RMPE changes sign concurrently with the local emergence of a new type of structure such as freezing. Since the concept of excess entropy can be applied to nonspherical particles, the zero-RMPE criterion has been successfully tested in rod suspensions at the nematic–smectic transition.[16] It would be interesting to see if the $s_2 \approx -4.5\ k_B$ criterion can also be applied to the freezing point of nonspherical particles. Moreover, by combining the s_2 criterion with the zero-RMPE criterion, we have $s = s_1 - 4.5\ k_B$, i.e., the entropy per particle becomes $4.5\ k_B$ lower than the entropy of an ideal gas when the system solidifies. Because s_2 only reflects the free volume but not the order in the structure, it cannot distinguish between crystalline and random closed-packed structures.[53] However it would be interesting to explore whether a critical value generally exists in glass transitions of monodispersed particles and freezing transitions of nonspherical or polydispersed particles where most other freezing criteria cannot be applied.

The area fraction is often used as the thermodynamic variable. This leads to different freezing area fractions for different systems as shown in Figs. 6 and 8. For softer particles, the freezing area fraction shifts to a larger value at 0.77 for r^{-12}-potential particles[4] and 1.188 for r^{-6}-potential particles.[44] In contrast, s_2 remains the same at a constant value of $-4.5\ k_B$ at the freezing points of different systems. Moreover the area fraction is ambiguous for soft particles, while s_2 defined in Eq. (8) has no ambiguity for different pair potentials. Hence we believe that s_2 could be a better thermodynamic variable than the area fraction. Nevertheless, s_2 directly reflects the two-body free volume which could be used as an alternative to the area fraction. When ρ or T is replaced by s_2 in Figs. 2–4 and 6, the melting point of different systems becomes approximately identical, see Fig. 9 as an example. Because the absolute value of χ_6 depends on the type of particles and the total sample area,[29,42,57] we scaled χ_6 to the same order in Fig. 9.

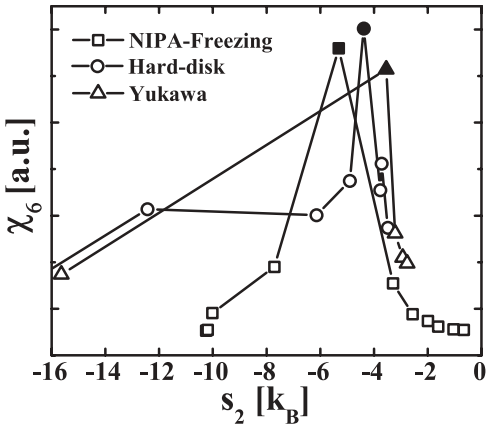

FIG. 9. The orientational susceptibilities as a function of two-body excess entropy s_2. All the peaks are located around $s_2 = -4.5\,k_B$, which corresponds the freezing transition. An arbitrary unit is used in χ_6 in order to compare the peak positions (i.e., the melting points) rather than the peak heights in different systems.

VI. SUMMARY

We observed two features at the freezing point in one experimental and two simulation systems with different interactions. Such features also exist in two melting experiments with different NIPA particle sizes and surface coatings.[29] Hence we suggest the two features could potentially be used as empirical 2D melting criteria.

The first feature is the bimodal distribution of the order parameter n_{6i}. The distribution profile of n_{6i} is sensitive to the volume fraction or the temperature, and can yield accurate freezing points. The bimodal profile can be resolved unambiguously with about ten times less statistics than are required by the other criteria. Moreover, n_{6i} can be accurately measured in a small sample area without finite-size ambiguity. At the freezing points, 50% of the particles in all five systems are solidlike. This feature can also be used to estimate the freezing point with even less statistics.

The second feature is that the two-body excess entropy per particle, s_2, reaches $-4.5 \pm 0.5\ k_B$ at the freezing point. s_2 can be obtained directly from macroscopic scattering measurements. Hence it is practically useful in molecular systems in which the microscopic information is difficult to obtain. Combining this s_2 criterion and the zero-RMPE freezing criterion, we found that a system freezes when the entropy per particle is $-4.5\ k_B$ lower than the entropy of an ideal-gas particle at the same density. Speculation of this critical value may cast light on solidification mechanisms. The universal $-4.5\ k_B$ suggests that the well-defined s_2 might be served as a better thermodynamic variable than the area fraction.

ACKNOWLEDGMENTS

This work was supported by the GRF (Grant No. 601208) from the Hong Kong SAR and the William Mong Institute of Nano Science and Technology at HKUST (Y.H.), the NSFC (Grant No. 10975063), the Fundamental Research Funds for the Central Universities (Grant No. lzujbky-2009-52) (Y.C.).

[1] H. Löwen, Phys. Rep. **237**, 249 (1994).
[2] U. Gasser, J. Phys.: Condens. Matter **21**, 203101 (2009).
[3] F. A. Lindemann, Physik. Z. **11**, 609 (1910).
[4] J. Q. Broughton, G. H. Gilmer, and J. D. Weeks, Phys. Rev. B **25**, 4651 (1982).
[5] H. Löwen, T. Palberg, and R. Simon, Phys. Rev. Lett. **70**, 1557 (1993).
[6] H. Löwen, Phys. Rev. E **53**, R29 (1996).
[7] S. Ranganathan and K. N. Pathak, Phys. Rev. A **45**, 5789 (1992).
[8] T. M. Truskett, S. Torquato, S. Sastry, P. G. Debenedetti, and F. H. Stillinger, Phys. Rev. E **58**, 3083 (1998).
[9] F. Moučka and I. Nezbeda, Phys. Rev. Lett. **94**, 040601 (2005).
[10] P. Giaquinta and G. Giunta, Physica A **187**, 145 (1992).
[11] G. P. Hoffmann and H. Löwen, J. Phys. Condens. Matter **13**, 9197 (2001).
[12] Z. -R. Wang, A. Alsayed, A. G. Yodh, and Y. Han, J. Chem. Phys. **132**, 154501 (2010).
[13] P. M. Reis, R. A. Ingale, and M. D. Shattuck, Phys. Rev. Lett. **96**, 258001 (2006).
[14] F. Saija, S. Prestipino, and P. Giaquinta, J. Chem. Phys. **113**, 2806 (2000).
[15] E. Lomba, J. L. López-Martín, H. M. Cataldo, and C. F. Tejero, Phys. Rev. E **49**, 5164 (1994).
[16] D. Costa, F. Saija, and P. Giaquinta, J. Phys. Chem. B **107**, 9514 (2003).
[17] F. Saija, J. Chem. Phys. **128**, 136101 (2008).
[18] M. Singh, H. Liu, S. Kumar, A. Ganguly, and C. Chakravarty, J. Chem. Phys. **132**, 074503 (2010).
[19] J. M. Kosterlitz and D. J. Tholuless, J. Phys. C **6**, 1181 (1973).
[20] D. R. Nelson, *Defects and Geometry in Condensed Matter Physics* (Cambridge University Press, Cambridge, 2002).
[21] M. A. Glaser and N. A. Clark, Adv. Chem. Phys. **83**, 543 (1993).
[22] S. T. Chui, Phys. Rev. Lett. **48**, 933 (1982).
[23] J. R. Savage and A. D. Dinsmore, Phys. Rev. Lett. **102**, 198302 (2009).
[24] P. Dillmann, G. Maret, and P. Keim, J. Phys. Condens. Matter **20**, 404216 (2008).
[25] C. A. Knapek, D. Samsonov, S. Zhdanov, U. Konopka, and G. E. Morfill, Phys. Rev. Lett. **98**, 015004 (2007).
[26] Y. Feng, J. Goree, and B. Liu, Phys. Rev. Lett. **100**, 205007 (2008).
[27] R. Pelton, Adv. Colloid Interface Sci. **85**, 1 (2000).
[28] A. M. Alsayed, M. F. Islam, J. Zhang, P. J. Collings, and A. G. Yodh, Science **309**, 1207 (2005).
[29] Y. Han, N. Y. Ha, A. M. Alsayed, and A. G. Yodh, Phys. Rev. E **77**, 041406 (2008).
[30] S. H. Behrens and D. G. Grier, Phys. Rev. E **64**, 050401 (2001).
[31] Y. Han and D. G. Grier, Phys. Rev. Lett. **91**, 038302 (2003).
[32] M. Polin, D. G. Grier, and Y. Han, Phys. Rev. E **76**, 041406 (2007).
[33] J. Baumgartl and C. Bechinger, Europhys. Lett. **71**, 487 (2005).
[34] J. C. Crocker and D. G. Grier, J. Colloid Interface Sci. **179**, 298 (1996).
[35] W. Qi, Z. Wang, Y. Han, and Y. Chen, J. Chem. Phys. **133**, 234508 (2010).
[36] W. B. Russel, D. A. Saville, and W. R. Schowalter, *Colloidal Dispersions* (Cambridge University Press, Cambridge, 1989).
[37] J. M. Caillol, D. Levesque, J. J. Weis, and J. P. Hansen, J. Stat. Phys. **28**, 325 (1982).
[38] K. Binder, Rep. Prog. Phys. **50**, 783 (1987).
[39] K. J. Strandburg, Rev. Mod. Phys. **60**, 161 (1988).
[40] J. Lee and K. J. Strandburg, Phys. Rev. B **46**, 11190 (1992).
[41] J. A. Zollweg and G. V. Chester, Phys. Rev. B **46**, 11186 (1992).
[42] H. Weber, D. Marx, and K. Binder, Phys. Rev. B **51**, 14636 (1995).
[43] C. H. Mak, Phys. Rev. E **73**, 065104 (2006).
[44] M. P. Allen, D. Frenkel, W. Gignac, and J. P. McTague, J. Chem. Phys. **78**, 4206 (1983).
[45] R. Pesché, M. Kollmann, and G. Nägele, J. Chem. Phys. **114**, 8701 (2001).
[46] A. Huerta, D. Henderson, and A. Trokhymchuk, Phys. Rev. E **74**, 061106 (2006).
[47] A. E. Larsen and D. G. Grier, Phys. Rev. Lett. **76**, 3862 (1996).
[48] A. H. Marcus and S. A. Rice, Phys. Rev. E **55**, 637 (1997).
[49] H. Raveché, J. Chem. Phys. **55**, 2242 (1971).
[50] A. Baranyai and D. J. Evans, Phys. Rev. A **40**, 3817 (1989).
[51] D. Wallace, J. Chem. Phys. **87**, 2282 (1987).
[52] Z. Yan, S. V. Buldyrev, and H. E. Stanley, Phys. Rev. E **78**, 051201 (2008).
[53] T. M. Truskett, S. Torquato, and P. G. Debenedetti, Phys. Rev. E **62**, 993 (2000).
[54] J. Errington and P. Debenedetti, Nature (London) **409**, 318 (2001).
[55] Y. Peng, Z. Wang, A. M. Alsayed, A. G. Yodh, and Y. Han, Phys. Rev. Lett. **104**, 205703 (2010).
[56] M. Schmidt and H. Löwen, Phys. Rev. Lett. **76**, 4552 (1996).
[57] R. Zangi and S. A. Rice, Phys. Rev. E **58**, 7529 (1998).